

Harnessing the Point-Spread Function for High-Resolution Far-Field Optical Microscopy

Xiangsheng Xie,¹ Yongzhu Chen,² Ken Yang,¹ and Jianying Zhou^{1,*}

¹State Key Laboratory of Optoelectronic Materials and Technologies, Sun Yat-sen University, Guangzhou 510275, China

²Key Lab of Numerical Controlled Technology, Guangdong Polytechnic Normal University, Guangzhou 510635, China

(Received 3 November 2014; published 24 December 2014)

The resolution limit of far-field optical microscopy is reexamined with a full vectorial theoretical analysis. A highly symmetric excitation optical field and optimized detection scheme are proposed to harness the total point-spread function for a microscopic system. Spatial resolution of better than $1/6\lambda$ is shown to be obtainable, giving rise to a resolution better than 100 nm with visible light excitation. The experimental measurement is applied to examine nonfluorescent samples. A lateral resolution of $1/5\lambda$ is obtained in truly far-field optical microscopy with a working distance greater than $\sim 500\lambda$. Comparison is made for the far-field microscopic measurement with that of a nearfield scanning optical microscopy, showing that the proposed scheme provides a better image quality.

DOI: 10.1103/PhysRevLett.113.263901

PACS numbers: 42.25.Ja

Introduction.—Enhancing the performance of optical microscopy is one of the most challenging research topics in the scientific community. [1] Intensive efforts have been made to achieve optical resolution beyond the diffraction limit during the past decade, among which the state-of-the-art far-field microscopic techniques such as stimulated emission-depletion microscopy [2], stochastic optical reconstruction microscopy [3], and structured illumination microscopy [4] were demonstrated, showing a spatial resolution better than 100 nm. While these powerful techniques are used mainly for microscopic optical images of specialized fluorescence labeling samples, other novel superresolution approaches [5–9] were successfully invented and demonstrated with special lenses or structures (superlens) to measure subwavelength hot-spots for nonfluorescence samples. The superlens-assisted microscopic technique can be categorized as so-called near-field optical microscopy [10].

Confocal laser scanning microscopy (CLSM) has been widely used because of its remarkable feature of obtaining optical images with high-resolution and depth selectivity. The imaging properties of a CLSM were best discussed in terms of a total point-spread function (PSF), which can be regarded as the product of excitation and detection PSFs. The resolution of CLSM was improved by shaping its total PSF, which is called “PSF engineering,” i.e., by modifying the spatial arrangement of the excitation and detection PSFs [11,12]. However, the lateral resolution is still restricted to about $\lambda/3$ by the diffraction limit under common conditions (air surrounded or oil immersed), without spatially modulating both excitation and detection PSFs.

Recent progress in the research of cylindrical vector beams provides a promising method for resolution enhancement of CLSM. A sharper focus can be generated in air [13], in oil immersion [14], and in solid immersion [15,16] with a spatially modulated radially polarized (RP)

beams. While the sharper focus is known to be equivalent to a narrower excitation PSF, the control of detection PSF is rarely studied. Moreover, with detection PSF for a tightly focused RP beam or azimuthal polarized (AP) beam, their doughnut shapes give rise to a dark-field image [17]. A sufficiently small pinhole placed before the detector can enhance the resolution by blocking the major z component of the light field [15], but the edge feature [17] and a poor signal to noise ratio deteriorate the image quality. A polarization mode converter was introduced to the CLSM to engineer the detection PSF with RP illuminations [18–20]. Higher-resolution imaging [378 nm full width at half maximum (FWHM) at 633 nm] comparing to that without the mode converter was performed. However, linear far-field microscopy without inserting structures or a lens in the vicinity of the sample is still restricted by the traditional resolution limit.

In this Letter, we propose and demonstrate a novel technique to enhance the optical resolution of a CLSM by harnessing both excitation and detection PSFs. A full vectorial theory of CLSM is applied for spatially modulated optical components and a new dyadic Green’s function is developed. High image quality with lateral resolution about $1/5\lambda$ is achieved experimentally, showing a good agreement with our theoretical analysis. The advantages developed in this work include applicability for a wide range of samples, no prior knowledge of the sample required, and less artifacts. The technique can be easily adapted to a conventional CLSM and to other spatially resolved systems, hence immediately enhancing their performances.

Theoretical model.—Theoretical studies on tight focusing are well presented in the form of the Debye-Wolf integrals [21]. Only the apodization function needs rewriting in the integral for a certain polarized incident beam [22]. Rigorous investigation on image formation in the CLSM system has been analyzed in the literature [11,23].

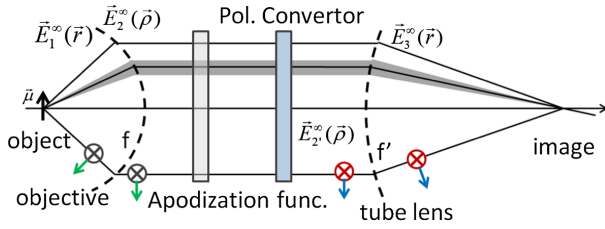


FIG. 1 (color online). Configuration for theoretical analysis of the PSF.

By inserting a polarization convertor, as shown in Fig. 1, the dyadic point-spread function \vec{G}_{PSF} , which describes the mapping of an arbitrarily oriented electric dipole from its source to its image, should be recalculated.

As shown in Fig. 1, the electric field at the reference sphere of the objective lens, derived from an electric dipole located at the focus, can be written as [11]

$$\vec{E}_1^\infty(\vec{r}) = \frac{\omega^2}{\epsilon_0 c^2} \vec{G}^\infty(\vec{r}, 0) \cdot \vec{\mu}, \quad (1)$$

where $\vec{G}^\infty(\vec{r}, 0)$ is the free-space far-field form of the dyadic Green's function, and $\vec{\mu}$ is the dipole momentum.

The electric field $\vec{E}_1^\infty(\vec{r})$ is collimated ($\vec{E}_2^\infty(\vec{r})$) by the objective lens, translated into a newly polarization distributed one $\vec{E}_2^\infty(\vec{r})$ by the polarization convertor, and focused by the tube lens as $\vec{E}_3^\infty(\vec{r}')$ at its reference sphere. The process can be mathematically expressed as

$$\vec{E}_2^\infty(\vec{\rho}) = \{t^S(\theta)[\vec{E}_1^\infty(\vec{r}) \cdot \hat{e}_\phi] \hat{e}_\phi + t^P(\theta)[\vec{E}_1^\infty(\vec{r}) \cdot \hat{e}_\theta] \hat{e}_\rho\} \sqrt{\frac{n_1}{n_2}} \frac{1}{\sqrt{\cos \theta}}, \quad (2)$$

$$\vec{E}_2^\infty(\vec{\rho}) = [\vec{E}_2^\infty(\vec{\rho}) \cdot \hat{e}_\rho] \hat{e}_x + [\vec{E}_2^\infty(\vec{\rho}) \cdot \hat{e}_\phi] \hat{e}_y, \quad (3)$$

$$\vec{E}_3^\infty(\vec{r}') = \{t^S(\theta')[\vec{E}_2^\infty(\vec{\rho}) \cdot \hat{e}_\phi] \hat{e}_\phi + t^P(\theta')[\vec{E}_2^\infty(\vec{\rho}) \cdot \hat{e}_\rho] \hat{e}_{\theta'}\} \sqrt{\frac{n_2}{n_3}} \frac{1}{\sqrt{\cos \theta'}}, \quad (4)$$

here $(\hat{e}_r, \hat{e}_\phi, \hat{e}_\theta)$ and $(\hat{e}_{r'}, \hat{e}_\phi, \hat{e}_{\theta'})$ are unit vectors of the spherical coordinate systems for the object and the image, respectively. $(\hat{e}_\rho, \hat{e}_\phi, \hat{e}_z)$ are unit vectors of the cylindrical coordinate system for the collimated light field. For a real polarization conversion device, the incident light field would be divided into RP and AP components, which would then be converted into two orthogonal LP beams, as shown in Eq. (3). The dyadic point-spread function then obtains a new form as

$$\vec{G}_{\text{PSF}}^{\leftrightarrow c}(\rho, \varphi, z) = -\frac{k' f}{8\pi f'} e^{i(kf - k'f')} \times \begin{bmatrix} \tilde{I}_{11} \cos \varphi & \tilde{I}_{11} \sin \varphi & i\tilde{I}_{00} \\ -\tilde{I}_{01} \sin \varphi & \tilde{I}_{01} \cos \varphi & 0 \\ 0 & 0 & 0 \end{bmatrix} \sqrt{\frac{n_1}{n_3}} \quad (5)$$

and the new integrals $\tilde{I}_{00} - \tilde{I}_{11}$ are defined as

$$\begin{aligned} \tilde{I}_{00}(\rho, z) &= \int_{\theta_{\min}}^{\theta_{\max}} P(\rho, \phi) (\cos \theta)^{1/2} \sin^2 \theta J_0(k' \rho \sin \theta f / f') \\ &\quad \times \exp\{ik'z[1 - 1/2(f/f')^2 \sin^2 \theta]\} d\theta, \\ \tilde{I}_{01}(\rho, z) &= \int_{\theta_{\min}}^{\theta_{\max}} P(\rho, \phi) (\cos \theta)^{1/2} \sin \theta J_1(k' \rho \sin \theta f / f') \\ &\quad \times \exp\{ik'z[1 - 1/2(f/f')^2 \sin^2 \theta]\} d\theta, \\ \tilde{I}_{11}(\rho, z) &= \int_{\theta_{\min}}^{\theta_{\max}} P(\rho, \phi) (\cos \theta)^{1/2} \sin \theta \cos \theta J_1(k' \rho \sin \theta f / f') \\ &\quad \times \exp\{ik'z[1 - 1/2(f/f')^2 \sin^2 \theta]\} d\theta, \end{aligned} \quad (6)$$

where $P(\rho, \phi)$ is the apodization function, which can modulate the detection PSF just as it was used to shrink the excitation PSF (for sharper focusing), and J_n is the n th -order Bessel function.

The Debye integration over the reference sphere of the tube lens can be carried out analytically and the electric field at the image region can be written as

$$\vec{E}_{\text{imag}}(\rho, \varphi, z) = \frac{\omega^2}{\epsilon_0 c^2} \vec{G}_{\text{PSF}}^{\leftrightarrow c}(\rho, \varphi, z) \cdot \vec{\mu}_n. \quad (7)$$

For a linear system with a sufficiently small pinhole, the electric field in the imaging region of a RP and an AP beam illumination becomes

$$\vec{E}_{\text{imag}}^R(\rho, \varphi, z) = \frac{\omega^2 \alpha k' f}{\epsilon_0 c^2 8\pi f'} e^{i(kf - k'f')} \sqrt{\frac{n_2}{n_1}} \sqrt{\frac{n_1}{n_3}} \times \begin{bmatrix} (i\tilde{I}_{00} I_{00} + \tilde{I}_{11} I_{11}) \hat{e}_x \\ 0 \hat{e}_y \\ 0 \hat{e}_z \end{bmatrix}, \quad (8)$$

$$\vec{E}_{\text{imag}}^A(\rho, \varphi, z) = \frac{\omega^2 \alpha k' f}{\epsilon_0 c^2 8\pi f'} e^{i(kf - k'f')} \sqrt{\frac{n_2}{n_1}} \sqrt{\frac{n_1}{n_3}} \begin{pmatrix} 0 \hat{e}_x \\ \tilde{I}_{01} I_{01} \hat{e}_y \\ 0 \hat{e}_z \end{pmatrix}, \quad (9)$$

respectively, where $I_{00} - I_{11}$ are the integrals for tightly focused beams [11].

For the RP beam, \tilde{I}_{00} and I_{00} are proportional to J_0 with a solid spot shape, and their values are much bigger than \tilde{I}_{11} and I_{11} , respectively, at a large incident angle (large θ). Modulation on the detection PSF $i\tilde{I}_{00}$ [in Eq. (4)] can further shrink the total PSF and enhances the resolution of the CLSM.

For AP beam, the polarization of the electric field in the imaging region is orthogonal to that of RP beam. \tilde{I}_{01} and I_{01} are proportional to J_1 with a doughnut shape.

Experiment.—An experimental setup based on a modified CLSM is established to verify the above theory, as shown in Fig. 2. The light path illustrated in green depicts the generation of a CV beam for the illumination and the one in orange is for the image forming, corresponding to Fig. 1. A linear polarized beam at 532 nm is passed through a liquid-crystal polarization converter (ARC optix, Switzerland) and an annular aperture before being focused by an oil objective lens [Olympus, X100, refractive index 1.52, numerical aperture (NA) 1.4]. The alignment of the experimental setup was carefully adjusted and the polarization purity of the RP beam was well inspected by a beam analyzing system [24]. To ensure the sharper focus, a double-knife-edge method [25] was applied to measure the spatial structure of the focus before the imaging process. After interacting with the sample, the reflected light is collected by the same objective lens and reversely passed through the annular aperture and polarization converter, and refocused by a tube lens into the pinhole of a fiber. Only one single polarization converter is required for the CV beam generation and the polarization conversion. There is no need to insert any structure or lens between the objective and the sample. The large working distance of the objective enables the system to resolve structures inside the sample or under a cover glass.

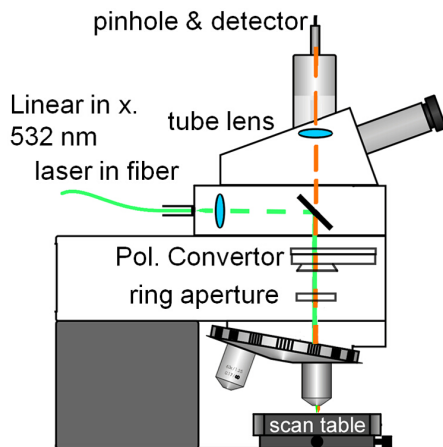


FIG. 2 (color online). Schematic of the experimental setup based on a CLSM.

The sample used for comparison is a latex projection pattern, which is an ideal test sample to determine the resolution of an imaging system. A monolayer of latex spheres with 581 nm diameter was used to shelter the substrate from the evaporated aluminium, resulting in a hexagonal array of aluminium triangular islands with ~ 200 nm side length separated by 290 nm, as shown in the inset of Fig. 3(a). The triangular islands cannot be resolved by a standard confocal microscope. A wide field view of the sample [Fig. 3(a)] merely indicates the alignment of the triangular islands, with a tilting angle $\sim 3^\circ$ to the scanning direction along the x axis. The transmission and reflection confocal images illuminated by a clear aperture LP beam are shown in Figs. 3(b) and 3(c) with a resolution of not better than 210 nm. The circular apertures corresponding to the removed latex spheres appear to be elliptic ones, with about 245 nm FWHM in the x direction and 210 nm in the y direction, because the PSF is elongated in the direction of polarization (x axis) of the focus. The reflection image [Fig. 3(c)] shows more artifacts, as the

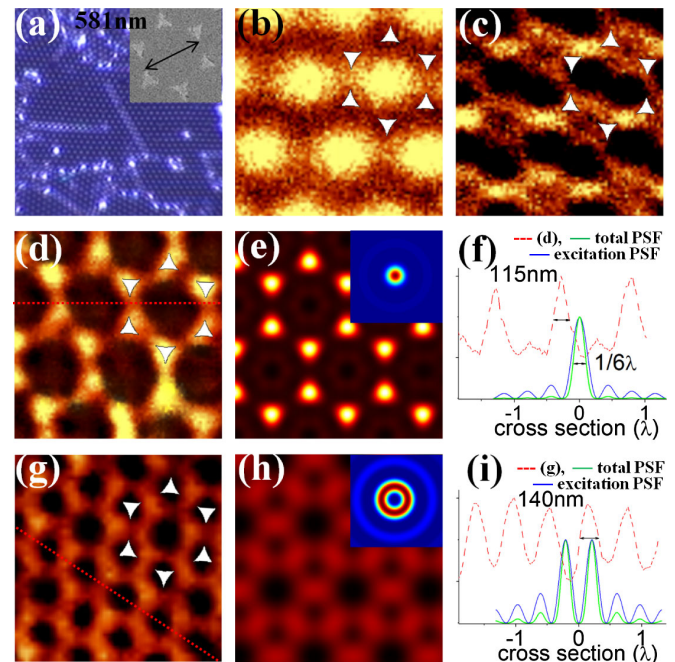


FIG. 3 (color online). Images of a latex projection pattern resolved by a standard confocal microscopy (the first row) and by the improved system with annular RP beam illumination (the second row) and annular AP beam illumination (the third row). (a) In wide field view. Inset: SEM image of the sample. (b) In transmission and (c) in reflection with a LP illuminating beam, where the inserted hexagonal arrays indicate the alignment of the triangular islands. (d) and (g) Experimental images in reflection. (e) and (h) Simulations with total PSFs shown in the inset. Typical translationally resolved measurement results (115 nm for RP and 140 nm for AP) shown as cross sections [(f) and (i)] through (d) and (g) (red dashed line). The simulated excitation PSFs (blue line) and total PSFs (green line) are shown in the same (f) and (i).

peanut-shaped dark pattern may be caused by plasmonic interaction between the triangle pairs and the light field. Each triangle pair forms a bowtie structure and gives rise to optical enhancement at the center of the gap due to the strong coupling between two nanotriangles. The smaller the angle between the polarization of the light field and the connection line of the triangle pair, the stronger the plasmonic resonance [26]. It is obvious that the microscopic imaging may be superimposed by strong artifacts as both the intensity profile and the polarization distribution of the focused light field contribute to the optical reflection.

Harnessing both the excitation PSF and the detection PSF is necessary for improving a CLSM on resolution as well as on its image quality. According to our calculation above, the excitation PSF can be improved if the polarization of the electric field has a cylindrical symmetry. The detection PSF can be converted by the system to form a similar profile as the excitation PSF. This results in a high contrast (sharper focus with suppressed sidelobes) total PSF, as shown in the inset of Figs. 3(e) and 3(h). The annular factor δ , defined as the ratio of inner and outer radii of the annular aperture, is 0.8. The pinhole radius r_{ph} is $12.5 \mu\text{m}$. For the RP illumination, the confocal image [Fig. 3(d)], corresponding to the original structure with resolved triangular islands, is well restored. The cross section of the image [Fig. 3(f)] shows that a resolution of about 115 nm ($\sim 1/5\lambda$) is achieved. Ideally, higher δ of a focused annular RP beam gives rise to sharper focus. In reality, the minimized spot was obtained for $\delta = 0.91$ because the diffraction effect has to be taken into account [14]. For a standard CLSM, the resolution (FWHM) is a function of the pinhole radius and $r_{\text{ph}} = 12.5 \mu\text{m}$ is sufficiently small to obtain the highest spatial resolution [11]. Nevertheless, r_{ph} should be smaller than $9 \mu\text{m}$ to achieve the required resolution calculated by integrating the intensity [referred to Eq. (7)] over the pinhole area. When $\delta = 0.91$ and $r_{\text{ph}} = 9 \mu\text{m}$, as shown in Fig. 3(f), the cross section of the total PSF is obviously sharper and has less sidelobes than that of the excitation PSF. A resolution of smaller than $1/6\lambda$ can be achieved, which corresponds to 67 nm for the illuminating wavelength at 405 nm . Further resolution enhancement can be achieved by using a lens with higher NA, e.g., a solid immersion lens with a refractive index of 3.5.

In contrast, without spatial light field modulation for the collected light beam, the image becomes blurred and irregular (not shown here) because of the reduced signal to noise ratio. Applying a sufficient large pinhole ($r_{\text{ph}} = 62.5 \mu\text{m}$) can restore the triangular islands, but the resolution is limited to the size of the excitation PSF [about 160 nm in Fig. 3(f)]. A circularly polarized (CP) beam is another promising light source for the CLSM, which does also provide a cylindrical symmetry. However, the RP beam is preferred as the spot size with a RP beam is found to be smaller than that with a CP beam at a high δ for the NA of the objective lens larger than 0.85 [27].

For AP illumination, the triangular islands turn into small dark spots in the image [Fig. 3(g)] since the total PSF is in doughnut shape while the circular apertures are resolved as bigger dark spots. It is interesting that the image still shows a resolution as high as 140 nm but it is in contrast different with the original array structure.

The original structure pattern can be retrieved according to a convolution theorem with the total PSF, as shown in Figs. 3(e) and 3(h). The simulation results show good agreement with the experiments in general. There are some substructures among the dark apertures in Fig. 3(d), which appear similar to the patterns in Fig. 3(g) with a location shift. The imperfect RP beam [24] and depolarization contributed by the sample scattering may all be contributing to this small deviation.

The interaction between the structured light field and structured matter [28] is a complex and promising issue. When compressing a light field into a nanofocusing spot, the structured light field, especially its polarization distribution, will affect the imaging process. Figure 4 shows the images resolved by a confocal microscopy with an annular LP beam and by an aperture NSOM. The simulated image (corresponding to the reflection image) illuminated by the annular LP beam [Fig. 4(a)] appears complementary to the experimental transmission image [Fig. 4(b)], but is different with the one in reflection [Fig. 4(c)]. The reason for the difference is that the annular aperture reduces the transverse light field component at the focus, but increases the longitudinal one. The strong electric field coupling is probably excited by the strong longitudinal light field. Intensity distribution of the light field at the apex of an aperture NSOM tip based on a standard system (AlphaSNOM, WITec GmbH) is simulated by means of

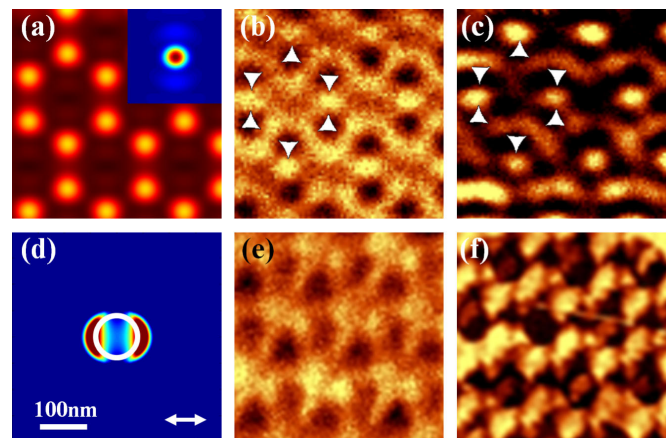


FIG. 4 (color online). Imaging analyses of a confocal microscopy (a)–(c) with a tightly focused annular LP beam and of an aperture NSOM (d)–(f). (a) Simulation image (in reflection) with total PSF shown in the inset. Experiment images in (b) transmission and (c) in reflection. (d) Intensity distribution of the light field at the apex of an aperture SNOM tip simulated by FDTD. (e) Transmission NSOM image and corresponding (f) AFM image.

finite difference time domain [29], as shown in Fig. 4(d). The light field cannot be confined within the aperture (90-nm diameter) and spreads into two sidelobes at the rim, hence degrading the resolving power of the NSOM. Complex electric field distribution at the apex and its coupling with the sample will further deteriorate the imaging quality of the NSOM, as shown in Fig. 4(e). This deterioration is still a problem of NSOM imaging and will probably be encountered in various applications. It is obvious that the confocal image illuminated by an annular RP beam has less anisotropy and better imaging quality.

In conclusion, we develop a full vectorial theory of CLSM with spatially modulated optical components. A new dyadic Green's function is deduced according to a realistic experimental configuration. A theoretical optical resolution beyond $1/6\lambda$ should be obtainable, giving rise to a routine sub-100 nm resolution for a truly far-field, visible linear optical microscopy. Lateral resolution of a confocal microscopy about $1/5\lambda$ is achieved experimentally by shrinking both the excitation and detection PSFs. We present experimental evidence that extreme care must be taken to understand the polarization properties for both the excitation and detection optical configuration and for sample polarization preferences when a high-resolution optical microscopy is applied for both far-field and near-field measurement. We believe that harnessing the PSF with highly symmetrical focused light fields for excitation and for detection should open up an avenue for sub-100 nm far-field linear, nonlinear, and time-resolved optical microscopy.

The authors thank U. Fischer from Muenster University for the sample preparation. This work is financially supported by the State Key Program for Basic Research of China (Grant No. 2012CB 921904), the National Natural Science Foundation of China (Grants No. 61205018 and No. 61475038) and the Fundamental Research Funds for the Central Universities.

*Corresponding author.

stszjy@mail.sysu.edu.cn

- [1] N. I. Zheludev, *Nat. Mater.* **7**, 420 (2008).
- [2] S. W. Hell and J. Wichmann, *Opt. Lett.* **19**, 780 (1994).
- [3] M. J. Rust, M. Bates, and X. Zhuang, *Nat. Methods* **3**, 793 (2006).
- [4] M. G. L. Gustafsson, *J. Microsc.* **198**, 82 (2000).

- [5] X. Zhang and Z. Liu, *Nat. Mater.* **7**, 435 (2008).
- [6] J. Rho, Z. Ye, Y. Xiong, X. Yin, Z. Liu, H. Choi, G. Bartal, and X. Zhang, *Nat. Commun.* **1**, 143 (2010).
- [7] I. I. Smolyaninov, Y. J. Hung, and C. C. Davis, *Science* **315**, 1699 (2007).
- [8] J. Y. Lee, B. H. Hong, W. Y. Kim, S. K. Min, Y. Kim, M. V. Jouravlev, R. Bose, K. S. Kim, I.-C. Hwang, L. J. Kaufman, C. W. Wong, P. Kim, and K. S. Kim, *Nature (London)* **460**, 498 (2009).
- [9] Z. B. Wang, W. Guo, L. Li, B. Luk'yanchuk, A. Khan, Z. Liu, Z. C. Chen, and M. H. Hong, *Nat. Commun.* **2**, 218 (2011).
- [10] E. T. F. Rogers, J. Lindberg, T. Roy, S. Savo, J. E. Chad, M. R. Dennis, and N. I. Zheludev, *Nat. Mater.* **11**, 432 (2012).
- [11] L. Novotny and B. Hecht, *The Principle of Nano Optics* (Cambridge University, Cambridge, England, 2006).
- [12] *Proceedings of SPIE, Wave-Optical Systems Engineering II*, edited by F. Wyrowski, Vol. 5182 (SPIE, Bellingham, WA, 2003).
- [13] R. Dorn, S. Quabis, and G. Leuchs, *Phys. Rev. Lett.* **91**, 233901 (2003).
- [14] L. X. Yang, X. S. Xie, S. C. Wang, and J. Y. Zhou, *Opt. Lett.* **38**, 1331 (2013).
- [15] R. Chen, K. Agarwal, C. J. R. Sheppard, and X. Chen, *Opt. Lett.* **38**, 3111 (2013).
- [16] A. Yurt, M. D. W. Grogan, S. Ramachandran, B. B. Goldberg, and M. S. Ünlü, *Opt. Express* **22**, 7320 (2014).
- [17] D. P. Biss, K. S. Youngworth, and T. G. Brown, *Appl. Opt.* **45**, 470 (2006).
- [18] W. T. Tang, E. Y. S. Yew, and C. J. R. Sheppard, *Opt. Lett.* **34**, 2147 (2009).
- [19] Y. K. Chen, D. G. Zhang, L. Han, G. H. Rui, X. X. Wang, P. Wang, and H. Ming, *Opt. Lett.* **38**, 736 (2013).
- [20] X. L. Wang, J. Chen, Y. N. Li, J. P. Ding, C. S. Guo, and H. T. Wang, *Phys. Rev. Lett.* **105**, 253602 (2010).
- [21] B. Richards and E. Wolf, *Proc. R. Soc. A* **253**, 358 (1959).
- [22] K. S. Youngworth and T. G. Brown, *Opt. Express* **7**, 77 (2000).
- [23] C. J. R. Sheppard and T. Wilson, *Proc. R. Soc. A* **379**, 145 (1982).
- [24] X. S. Xie, H. Y. Sun, L. X. Yang, S. C. Wang, and J. Y. Zhou, *J. Opt. Soc. Am. A* **30**, 1937 (2013).
- [25] X. S. Xie, L. Li, S. C. Wang, Z. X. Wang, and J. Y. Zhou, *AIP Adv.* **3**, 022110 (2013).
- [26] P. J. Schuck, D. P. Fromm, A. Sundaramurthy, G. S. Kino, and W. E. Moerner, *Phys. Rev. Lett.* **94**, 017402 (2005).
- [27] G. M. Lerman and U. Levy, *Opt. Express* **16**, 4567 (2008).
- [28] N. M. Litchinitser, *Science* **337**, 1054 (2012).
- [29] Y. Z. Chen, X. S. Xie, Y. Y. Li, and J. Y. Zhou, *Appl. Phys. Lett.* **100**, 051104 (2012).